JOURNAL OF MATERIALS SCIENCE **40** (2005) 5829–5837

Polymeric foam behavior under dynamic compressive loading

P. VIOT, F. BEANI, J.-L. LATAILLADE
LAMEFIP, ENSAM de Bordeaux, Esplanade des arts et métiers, 33405, Talence Cedex, France

Polymeric foams are commonly used in many impact-absorbing applications and thermal-acoustic insulated devices. To improve their mechanical performances, these structures have to be modeled. Constitutive equations (for their macroscopic behavior) have to be identified and then determined by appropriate tests.

Tests were carried out on polypropylene foams under high strain rate compression. In this work, the material behaviour has been determined as a function of two parameters, density and strain rate. Foams (at several densities) were tested on a uniaxial compression for initial strain rates equal to 0.34 s^{-1} and on a new device installed on a flywheel for higher strain rates. This apparatus was designed in order to do stopped dynamic compression tests on foam. With this testing equipment, the dynamic compressive behaviour of the polymeric foam has been identified in the strain rate range [$6.7.10^{-4}s^{-1}$, $100s^{-1}$].

Furthermore, the sample compression was filmed with a high speed camera monitored by the fly wheel software. To complete this work, picture-analysis techniques were used to obtain displacement and strain fields of the sample during its compression. Comparisons between these results and stress-strain responses of polypropylene foam allow a better understanding of its behaviour. The multiscale damage mechanism, by buckling of the foam structure, was emphasised from the image analysis.

1. Introduction

Polypropylene foams are used in many passive security applications such as packaging of fragile components (electronic devices etc.) or in various protective products like helmets or knuckle pads used by sportsmen, motorcyclists or construction workers. For sport helmets, which have been the basis of this study, these foams are used as padding material, placed between the external plastic shell of the helmet and the fine comfortable foams in contact with the sportsman's head. If the rigid shell prevents -or limits- blunt object penetration during a shock, the function of polypropylene foams is to absorb the impact energy in order to protect the sportsman's head.

To improve the safety performances of this type of material, these structures have to be modeled in dynamic F.E. software. However, for this design approach, it is necessary to know the mechanical characteristics of each material used in the product. Thus, the first aim of this work has been to identify the polypropylene foam behavior under dynamic loadings. Furthermore, because the state of stress imposed on foam structure during an impact is principally compression, it seems obvious to identify the cellular material response under dynamic compression.

Gibson and Ashby [1] showed that polymeric foam behavior is commonly elasto-plastic. During a compression test –axis y-, the stress evolution versus strain constitutes three stages: an elastic behavior followed by a plastic plateau stress σ_{pl} characteristic of the material's progressive damage. The final one is the porous material densification. Moreover, this behavior depends on the foam density and the strain rate (see [2, 3]). The identification of rheological parameters as a function of this second parameter $\dot{\varepsilon}_y$ can be obtained by using different testing machines. If conventional testing machines are used for quasi-static compression tests, specific devices have to be used at high strain rates. For example, for strain rates $\dot{\varepsilon}_y$ higher than $1000s^{-1}$, it is necessary to use Kolsky – Hopkinson techniques (see [4–6]). However, intermediate strain rates interest us more particularly since they correspond better to the strain rates observed during an impact on protective structures such as helmets.

For these strain rates, drop towers are often used to estimate material behavior or to verify performances of a complex structure loaded by a projectile impact [7]. However, the impactor speed is not constant and the strain rate varies considerably, as it depends on the response of the structure. For this reason, this device is not appropriate and a new testing apparatus has been developed on a fly wheel. Results obtained with this compression device are presented in this paper.

0022-2461
DOI: 10.1007/s10853-005-4998-5

If the first objective of this work was obviously to complete the identification of foam behavior over a large range of strain rate, a complementary study was also carried out in order to reveal material deformation mechanisms at mesoscopic scale. For the first time, optic measurement techniques used during dynamic tests have shown strain fields are non homogenous (foam damage is obtained by local cell wall buckling). This article emphasizes foams can not be studied only at macroscopic scale like homogen material, given that high gradients of strain measured during impact implicate a mesoscopic modeling of the material considered like a structure.

2. Experimental program

2.1. Devices and machines

Two testing machines were used to test polypropylene foam samples. The first one is an electro-mechanical testing machine -Adamel-, with a maximum force of 10 KN. The maximum compression speed is 500 mm/min, with the initial strain rates reaching 3.4×10^{-1} s^{-1} at a sample height of 24 mm. The first tests done on this machine enabled us to identify the foam behavior at low strain rates and also to predict the material response at higher strain rates in order to design a new dynamic compression device. This new device was used on a fly wheel to load foam samples at strain rates up to 40 s^{-1}.

2.1.1. Dynamic compression on fly wheel

The fly wheel was developed at the LAMEFIP Laboratory (see Lambert [8]). It consists of a heavy metallic wheel with a diameter of 1 m, a mass of 617 kg, and an inertia moment of 77 kg·m^2, carrying a hammer. An asynchronous motor accurately controls the angular frequency of the wheel. This apparatus was initially designed to carry out dynamic tensile tests on light metal alloys. It is used by clamping a sample to a pendular device, by a pivot with the engine framework, the position which is controlled by a pneumatic jack (Fig.1). During the test, when the hammer is detected by an optical sensor, the jack pushes the pendular device against the wheel. An anvil fixed at the bottom end of the sample is grabbed by the wheel hammer, which initiates the tensile test on the sample. The test is stopped when the sample cracks.

A new device for carrying out dynamic compressions on cellular materials was specially developed in our research utilizing this technical principle [9]. It was designed to apply compression on small polymeric foam samples, the cube size is less than 30 mm, and to stop the compression when the force reaches a defined value. The interruption of the test at a predetermined loading is interesting for two main reasons: firstly, the state of a foam sample, i.e. shape and microstructure, can be visualized after the test and for a damage level, and secondly, it is necessary to limit the maximum force to avoid any damage on the parts of the testing apparatus like the compression device, wheel hammer, motor, etc.

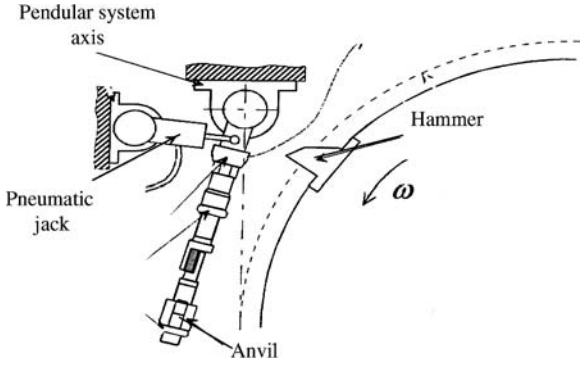

Figure 1 Scheme of the fly wheel and compression device

The new device includes two subsets, a module of compression and a positioning module (Fig. 2). The latter consists of tubular parts (A and B) assembled by threading to adjust the position of the sample. Moreover, a tube (A) is equipped with 4 strain gauges to determine only the compressive force F_y. The compression module consists of an anvil and a compression block (C). The anvil is guided in translation by a tube (B) and the compression block (C) is fixed on the same tube (B) via a fusible pin (D). The foam sample is compressed between the anvil and the plateau of the compression block. During the test, the anvil is grabbed by the wheel hammer and it determines the deformation level on the sample. When the compressive force reaches a threshold value, the fusible pin (D) is sheared and the subset of compression is ejected. The pin is made of polycarbonate, with two diameters (8 and 10 mm) used to reach two maximum values of compression (3000 and 4500 N). Its deformation is very weak during the test and its fracture is brittle.

Measured parameters are the axial force $F_y(t)$ and the angular velocity ω of the wheel. The force $F_y(t)$ is computed from the strain measurement of the tube (A) after a preliminary calibration. The axial stress $\sigma_{yy}(t)$ at time t is obtained from this result and the section S(t). The evolution of this last data can not be known precisely. However Gibson and Ashby [1], and Avalle [10] have shown that the Poisson ratio of polymeric foams is weak and can be considered as zero. The test results that we have obtained on polypropylene foam at several strain rates confirm this hypothesis. So, the axial stress is calculated from the axial force and the initial section $S(t_0)$. The axial strain ε_{yy} and the strain rate $\dot{\varepsilon}_{yy}$ are calculated from the angular velocity of the wheel and the initial height of the sample ($h_0 = 24$ mm) using Equation 1:

$$\varepsilon_{yy}(t) = \ln\left(\frac{h(t)}{h_0}\right) = \ln\left(\frac{h_0 - R.\varpi.t}{h_0}\right) \qquad (1)$$

at a time, R being the wheel radius.

2.2. High speed camera

A Phantom V4 high speed camera was added to the compression mechanical device, in order to firstly verify if the compression velocity was constant during the loading and secondly to estimate the strain rate field of the cellular material. Its maximum resolution is 512 × 512 pixels at 1000 images per second (coded in 10 bits). For these tests, the optimal setting was 2600 frames per second at a resolution of 128 × 512 pixels.

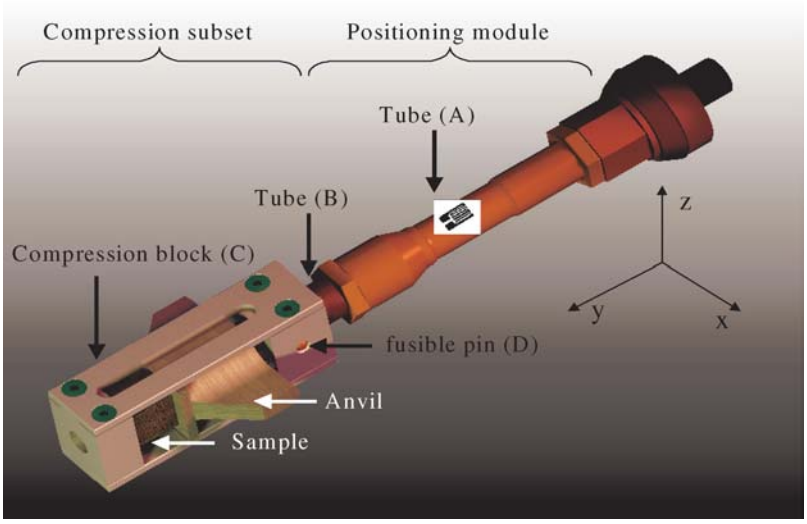

Figure 2 Computer image of compression device.

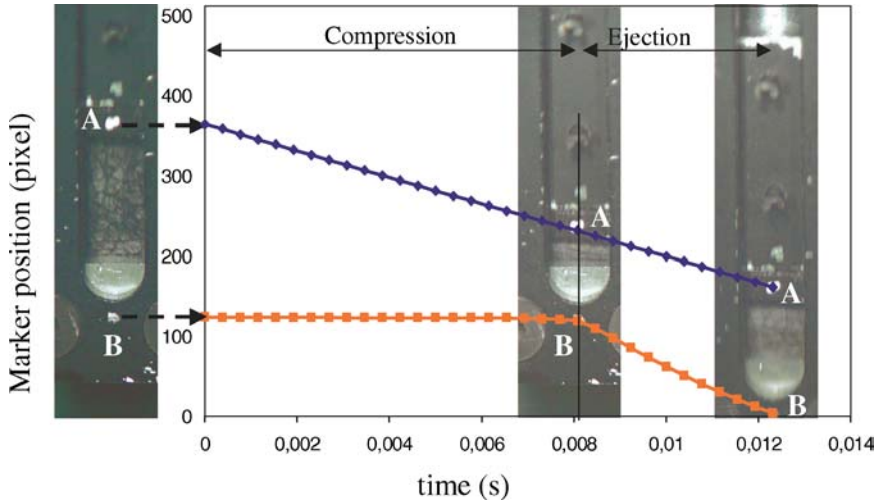

Figure 3 Displacements (in pixels) of white markers painted on mobile punch (blue curve) and on compression block (red curve) as a function of time during both test steps (compression and ejection).

The main difficulty for this video recording lies in the correct adjustments of settings such as depth of field, obturation time, and lighting, in order to ensure luminous and clear images of foam samples compressed inside the pendular device as well as mobility during the test. The settings are adjusted when the fly wheel is stopped and with the compression device in impact position against the wheel. The maximal exposition time is 167 μs at 2600 frames per second. This setting would be sufficient if the sample deformation is homogeneous, but we have noted a strong localization of sample strain. Thus, the exposition time had to be decreased to 87 μs in order to avoid any blur in the high strain zone.

With such a short exposure time, a powerful lighting source was necessary. Two projectors, of 1500 Watts each, and two additional spotlights with optical fiber were positioned in order to obtain a homogeneous luminosity, a good contrast and a sufficient depth of field compatible with this very short exposure time. The spotlights are switched on just before the compression in order to avoid a temperature increase in the sample, which could modify its mechanical properties.

2.3. Image analysis

The evolution of strain rate, assumed constant during the compression, has been estimated by the displacement measurement of the white markers [11]. Two markers A and B in Fig. 3 were painted on the mobile anvil and on the lower compression plate. The images, saved in 256 grey levels, are converted by binarisation into black and white images. The binarisation level has to be chosen, so that the white markers show up clearly on the black background. The barycentre displacement of each marker is calculated in pixels, with a good accuracy of 1/16th pixels. A preliminary calibration between the real position of markers (in mm), and their positions in numerical pictures (in pixels) is necessary. With the picture height and initial gap between the two markers being 230 pixels and 30 mm respectively, the displacement accuracy is 8 μm. The displacement of these points calculated as a function of time (Fig. 3) clearly shows the two test steps.

Compression step: the displacement of the anvil marker (point A, blue curve) is imposed by the wheel hammer whereas the point B displacement is very weak (red curve), corresponding to the compression device

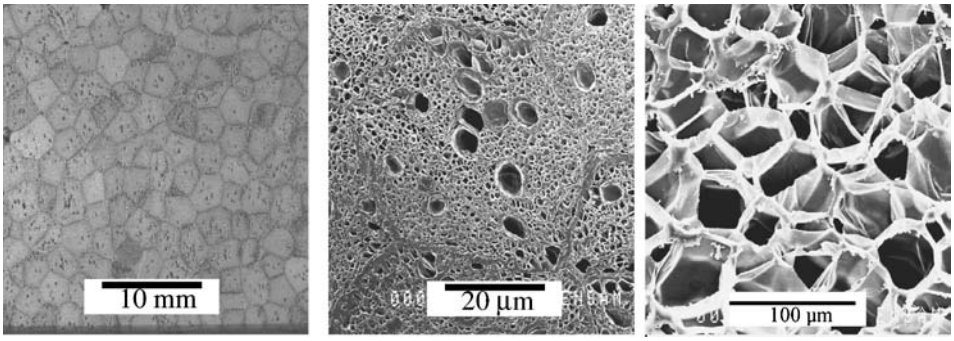

Figure 4 (a) Visual aspect of the polypropylen foam $p = 1$ (80 kg/m^3). (b) and (c) SEM picture of the foam mesostructure.

deformation. From these image analysis, one can verify that the displacement rate is constant during the compression step.

Ejection step: the point A displacement is always imposed by the hammer. But, since the fusible pin is sheared, the lower plate displacement results from the rigid compression device movement and from the sample spring back.

The pictures are also analyzed using image-correlation techniques in order to reveal any discontinuities on the strain field. Displacement and strain fields are calculated between two successive frames. A virtual squared grid is defined on the first picture, and found on the second picture by correlation (see [12, 13]). The displacement calculation accuracy can reach 0,01 pixels. The use of the digital image correlation technique gives the best results with pictures showing a high grey level. Thus, the sample surface is usually prepared in order to obtain a grey random speckle by spraying fine white particles on the sample dark surface. With the investigated polypropylene foam, this preparation is not necessary because the sample aspect is naturally black and white speckled (Fig. 4a).

2.4. Material

Polypropylene foam structure is multi-scale with agglomerated polygonal grains (diameter of 2 millimeters) easily seen in Figs. 4a and b. The grain wall thickness is about ten micrometers. The micrographic analysis reveals that each grain is constituted by small closed cells organized in a random way (Figs. 4b and c). Cell diameters are variable, from 10 micrometers for the smaller cells up to 60 micrometers for the larger ones. However, the cell wall thickness seems constant and less than 1 micrometer.

The foam structure does not seem to present any particular orientation at macro or mesoscopic scales. The hypothesis of isotropic behavior has been considered and was verified through preliminary compression tests [9]. These tests have also made it possible to optimize the sample dimensions. The volume $24\times24\times24$ mm^3 has been chosen in order to reduce the density variation in the sample but also to be a representative elementary volume of the inhomogeneous material (more than 200 expanded can be counted in a sample section polypropylene grains, each one made up of hundreds of closed cells).

3. Results

The foam behavior was studied as a function of two parameters, foam density and strain rate imposed during the loading.

3.1. Influence of the density

The sensitivity of the foam behavior to the density has been evaluated on the fly wheel by imposing impact on samples of four volumic masses (70, 80, 90 and 100 kg/m^3). Results of Fig. 5 were obtained at a strain rate

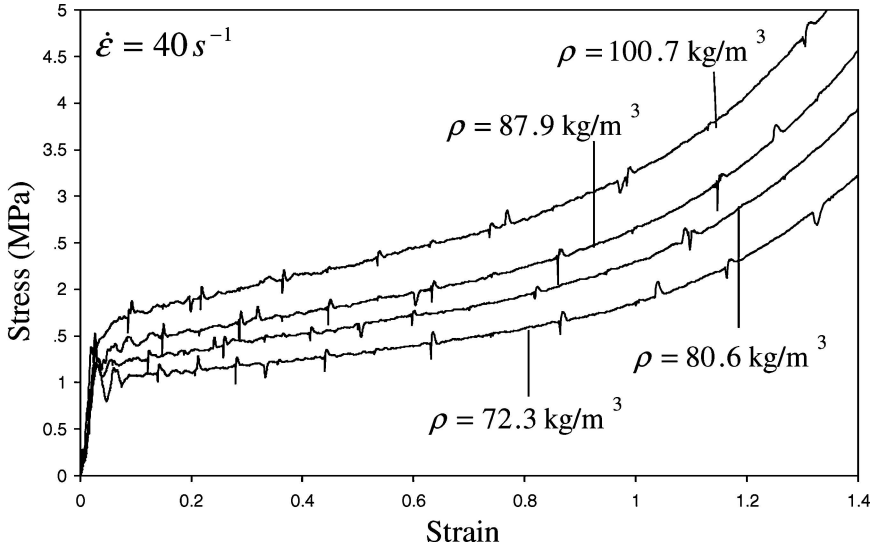

Figure 5 Uniaxial stress-strain curves of polypropylene foams in dynamic compression; influence of the foam density at high strain rate ($\dot{\varepsilon} = 40\,s^{-1}$).

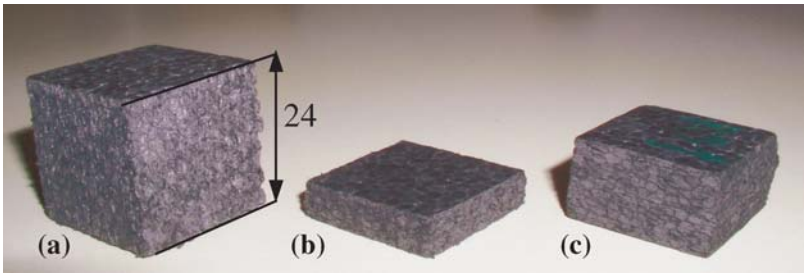

Figure 6 Effect of the strain rate on the sample shape after compression: picture of samples before test (a), after quasistatic compression (b) and after dynamic loading (c), (height in mm).

of $\dot{\varepsilon} = 40\,\mathrm{s}^{-1}$ (the hammer speed is then 1 m(s). These results are representative of all the tests carried out at different impact rates (0.9 m/s, 1 m/s, 2.5 m/s, and 5 m/s).

The curves in Fig. 5 are obtained directly from the sensor force responses. They are not fitted, and these results can be considered correct even if weak cyclic perturbations can be noted (due to the electromagnetic noise of the asynchronous motor). These curves present a similar evolution: first an elastic stage followed by a plastic plateau, and finally a rise in stress during the foam densification. For any strain rate, it clearly appears that an increase in density involves a rise of the plateau stress. The point is that a higher density obviously involves a higher quantity of polypropylene, because either the cell number is more significant or the cell walls are thicker. In any case, it seems logical that the higher the density of the foam is, the more resistant it is.

3.2. Influence of the strain rate

The strain-rate dependence of the foam behavior has been evaluated on samples of the same density by using both testing machines; the electromechanical press for strain rate lower than $0.3\,\mathrm{s}^{-1}$, and the flywheel for strain rate higher than $40\,\mathrm{s}^{-1}$.

The influence of the strain rate is immediately visible on the sample shape after compression. Fig. 6 displays samples before the test (a), after a quasi static compression (b) and just after dynamic loading (c). For these samples, the compression rate imposed during the test is the same, but the elastic responses during the unloading path are completely different. During the quasi static compression, one can suppose that air bubbles, trapped inside foam cells, may be released during this time. On the contrary, most of them stays inside cells during a dynamic loading and imposes a strong spring back of the sample.

The strain rate effect is also visible on the foam response. Fig. 7 shows the stress–strain curves of the tests carried out on samples of density 90 kg/m^3. There is an increase in the plateau stress with the rise in strain rate. This influence is verified for the four densities.

Curves obtained from flywheel tests at strain rates higher than $100\,\mathrm{s}^{-1}$ have strong oscillations attenuating during testing. This phenomenon, inherent in impact loading and already observed on other machines such as drop weight towers, is due to the impact wave propagation through the sample, the compression device and the machine. The tests carried out with the flywheel, at strain rate of $200\,\mathrm{s}^{-1}$ and more, have stronger oscillations, making it the evaluation of the plateau stress difficult. This device can be improved by using a Hopkinson bar already implemented on the flywheel device (see Lambert [8]).

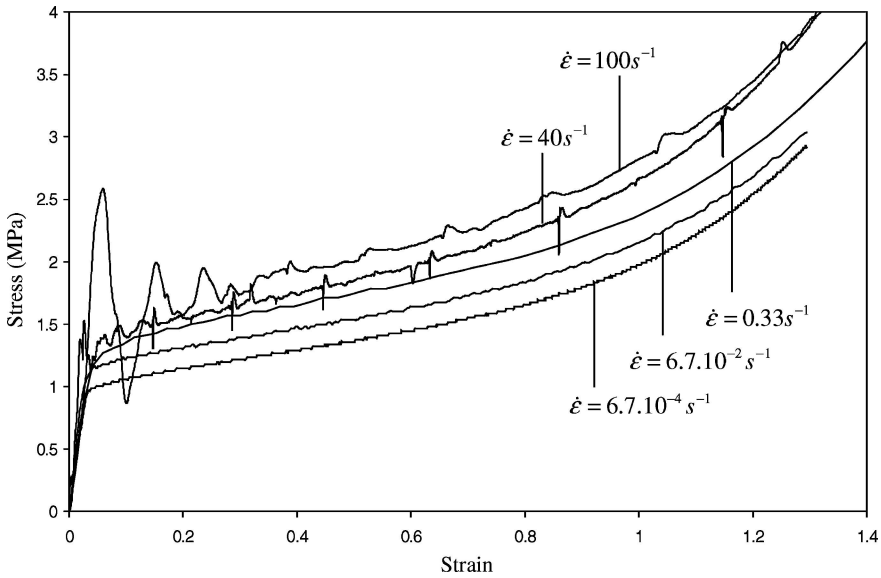

Figure 7 Influence of the strain rate on the foam response (density 90 kg/m^3); stress-strain curves obtained on the two testing machines.

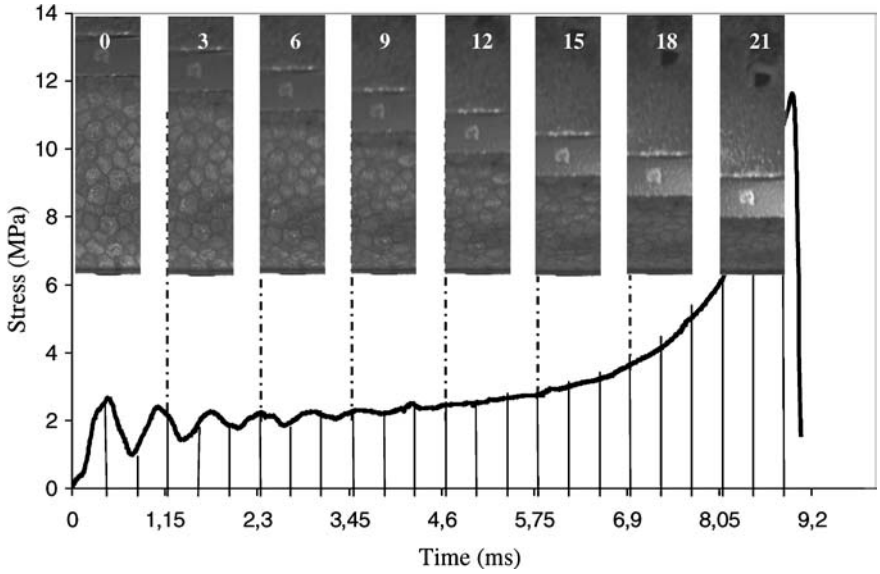

Figure 8 Evolution of the uniaxial stress and sample deformation picture as a function of time during dynamic compression (test parameters: volumic mass $p = 100$ kg/m^3 and initial strain rate $\dot{\varepsilon} = 100\,\mathrm{s}^{-1}$).

3.3. Identification of the strain field

The global behavior of the polypropylene foam is now identified over a large range of strain rates. If in the literature, one can find that in compressive stress states, foams fail by elastic or plastic buckling, the authors do not present the damage evolution during dynamic compression and no one has defined the strain fields. However, this study seems necessary in order to better understand the failure mechanisms of the material and also to define more precisely the local behavior of the cellular structure. The use of a digital image correlation technique made it possible to answer these points.

The test filmed at 2600 frames per second gave 24 pictures during the dynamic loading (Fig. 8). The first image (number 0, Fig. 8) corresponds to the uncompressed state of the material. From test image 3 to image 18, the sample deformation state can be visualized during the plastic plateau. On these images, it is easy to identify the zone where the cell buckling started (the darker zone close to the sample center). A strong localization of the deformation is visible in this area, whereas the polypropylene grains located in the upper part of the sample do not seem deformed. At the plastic plateau end, most of the cells were damaged. Test images 18 (and following) allow the visualization of the material deformation during its densification.

These first comments were confirmed with image analysis.

The displacements d_x and d_y along x and y direction respectively of image pixels were calculated in pixel and between two successive images i and $i+1$. For instance, Figs. 9a and b show respectively the displacement fields d_x and d_y calculated between images 3 and 4 (time $t = 1{,}15$ ms). At this time, along the loading direction y, displacements d_y are constant on the upper part of the sample and correspond to a rigid

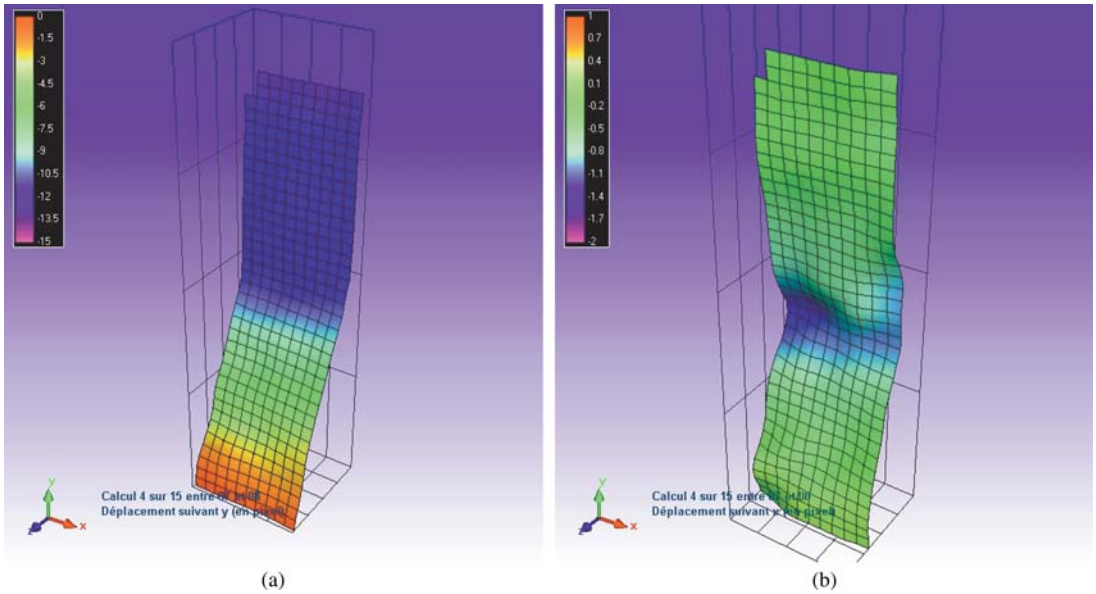

Figure 9 (a) Displacement field d_y and (b) displacement field d_x calculated from frames 6 and 7 (results in pixels).

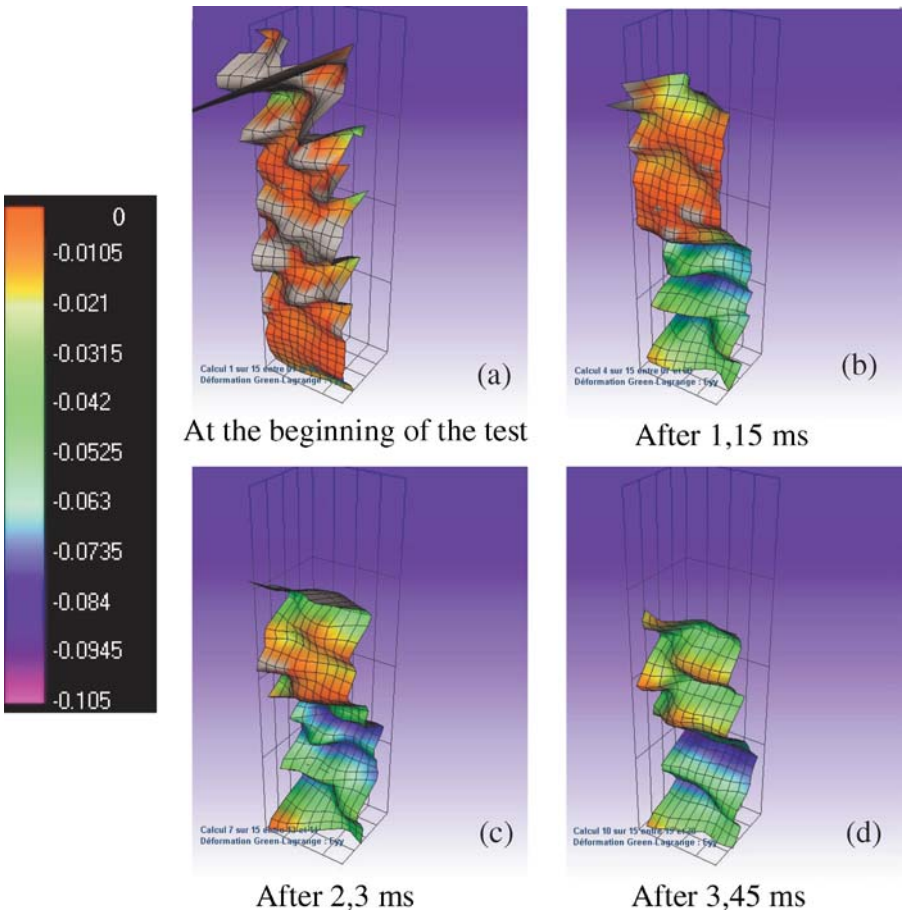

Figure 10 Evolution of strain field ε_{yy} as a function of time.

solid displacement. On the lower part, d_y field tends linearly to zero (the sample being put in the rigid compression block). Regarding the d_x displacement field, it is obviously very weak (Fig. 9b).

These results enable the calculation of the strain field $\varepsilon_{yy}, \varepsilon_{xx}$ and ε_{xy} between two successive times (384 μs). The calculation accuracy of the strain field can not be precisely estimated. It depends on different parameters such as image quality, homogeneity of the lighting during the test and analysis algorithm performances. However, if the displacement calculation accuracy can reach 0,01 pixels, the accuracy on the strain calculation can be evaluated close to 10^{-3} (the calculation grid size chosen to obtain the strain field is 10 pixels).

During the elastic step (Fig. 10a), the strain field ε_{yy} obtained from the analysis of the first two frames is obviously weak, because these strain values are close to the accuracy of image analysis. These results have to be considered with caution. On the contrary, during the plastic plateau, strains ε_{yy} are high and can be analyzed with assurance. Obtained after 1,15 ms between test frames 3 and 4, and after 2,3 ms between test frames 6 and 7, strain fields ε_{yy} show strong localization which corresponds to the local foam damage, the strain gradient reaches – 0.084 (Figs. 10b and c). Above this layer, strains ε_{yy} are weak and close to those obtained in elastic phases, whereas in the lower part, strains ε_{yy} are significant and include significant waves perpendicular to the loading direction; the undulation height is close to 0,04. During the plastic plateau, foam failure makes progress near these horizontal layers and the local strain gradient becomes less significant. In all of the dynamic compression tests, this phenomenon was noticed: a foam band is damaged and the material collapse propagates in the vicinity of this layer. However, the position of this damage layer is random whereas its orientation is usually perpendicular to the loading direction.

Hence, after 3,5 ms (Fig. 10d), the state of strain becomes more homogeneous. Most of the foam cells are crushed and the foam behavior tends towards the response of dense material. In the same way, the displacement derivation allows a quantification of the strain fields ε_{xx} and ε_{xy}. Since the accuracy on the strain is close to 10^{-3}, the results on the strain fields have to be analyzed carefully. However, figures seem to show that the strain fields ε_{xx} and ε_{xy} calculated during the elastic step (Figs.11a and Fig. 12a) and plastic plateau (Figs.11b and 12b) remain uniform during all the compression, and are independent of the material damage state. Concerning ε_{xx}, these calculations do not enable us to reveal an evolution of this strain ε_{xx} according to ε_{yy}. This dynamic compression result corroborates quasi static compression results which indicate that the Poisson ratio of polymeric foam is zero [1, 2].

To conclude, a micrographic analysis of compressed samples was achieved in order to evaluate the damage state of the foam. The SEM picture (Fig. 13) shows residual deformation at different scales. At the mesoscopic scale, one can observe many bands of plastically deformed cells, with their fine walls buckled under the

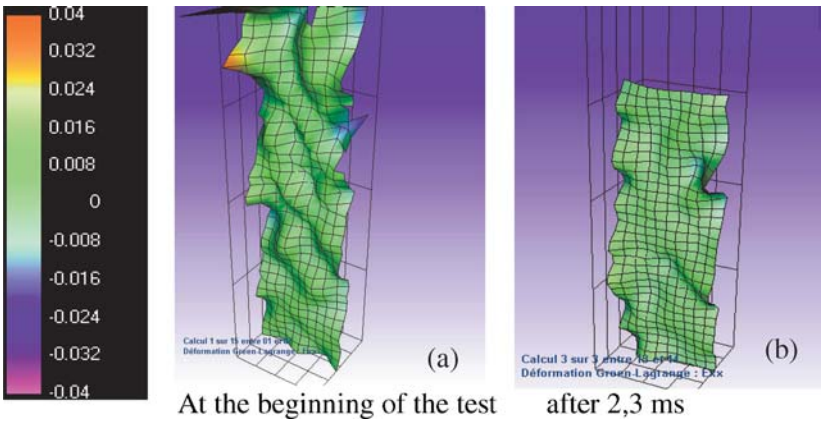

Figure 11 Evolution of strain ε_{xx} as a function of time.

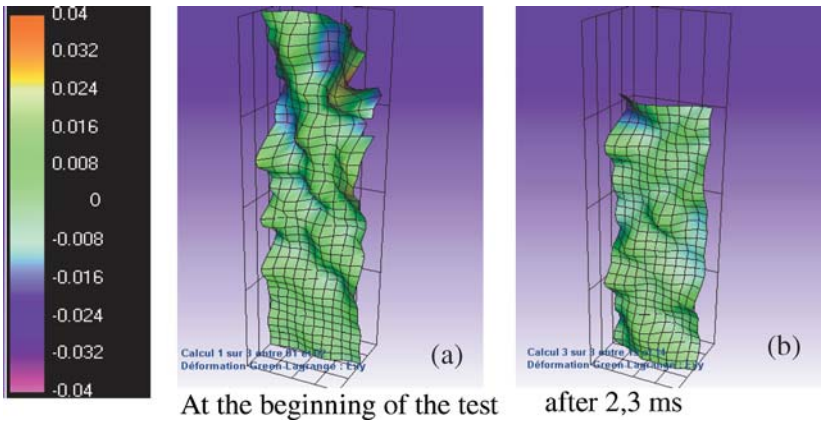

Figure 12 Evolution of strain ε_{xy} as a function of time.

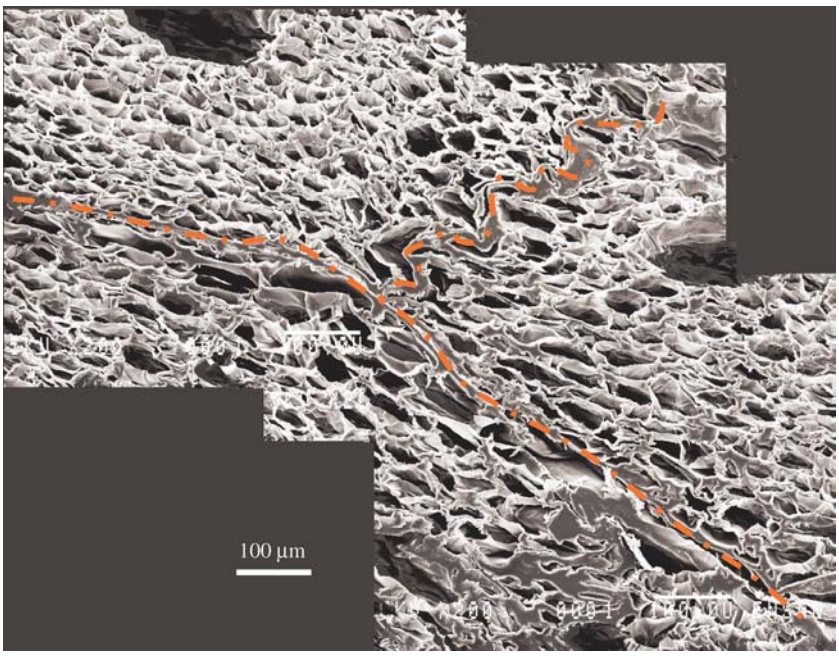

Figure 13 Scanning Electron Microscopy (SEM) of foam sample after impact.

loading effect. Other bands, yet intact, have kept their initial polygonal shapes. This damage mechanism, by local buckling of cell walls, explains the stress-strain curves; the plastic plateau corresponds to the buckling propagation of foam cells, propagation which develops from layers perpendicular to the loading direction.

At a larger scale, polypropylene grain walls have been also deformed by buckling. The complex shape of these buckled walls depends principally on the local stiffness of near by cells. The failure mechanism can be thus considered multiscale, mesoscopic for the fine wall buckling and macroscopic concerning the damage of large grain walls.

4. Conclusion

The new dynamic compression device makes it possible to estimate the evolution of the axial stress response of the cellular material as a function of imposed axial strain rate. High speed camera techniques and associated analysis were implemented on this apparatus in addition to the usual sensors.

Dynamic compression tests have shown that the polypropylene foam response includes an elastic step followed by a stress plateau during witch the material is progressively damaged. The final step is the foam densification. The influence of two parameters density and strain rate on the foam behavior the was underlined. More precisely, one could observe that the rise in density involves an increase in the stress plateau. The influence of the strain rate on the material response was also shown, with an increase in the stress threshold with the strain rate.

The complementary analysis of these tests by the use of digital image correlation techniques has shown that the foam damage appears severe on a fine layer perpendicular to the loading direction and develops from this band. The deformation mechanism of fine wall cells and larger expensed grain walls is mainly buckling. So, the damage mechanism is multi scale.

Some current research working on this type of polymeric foam is steering towards the modeling of the microscopic cell behavior in order to evaluate the macroscopic foam response. However, the multiscale structure of this cellular material also needs to take into account the stiffening effect of the macroscopic grain walls. This multi scale modeling has to be started and these experimental results obtained in dynamic compression already make it possible to complete the data base concerning this material.

References

1. L. GIBSON and F. ASHBY, "Cellular Solids. Structures and Properties", (Cambridge Solid State Science Series, 1997), Chap. 5, ISBN 0–521-49911-9.
2. J. ZHANG, N. KIKUCHI, V. LI, A. YEE and G. NUSCHOLTZ, "Constitutive Modeling of Polymeric Foam Material Subjected to Dynamic Crash Loading" **21**(5) (1998) 369.
3. M. MAIER and U. HUBER *et al*., "Recent Improvements in Experimental Investigation and Parameter Fitting forEellular Materials Subjected to Crash Loads". *Comp. Sci. Techn.* **63**(14) (2003) 2007.
4. W. CHEN, F. LU and N. WINFREE, "High-strain-rate compressive behavior of a rigid polyurethane foam with various densities". *Exper. Mech.* **42**(1) (2002).
5. T. THOMAS, H. MAHFUZ, L. CARLSSON, K. KANNY and S. JEELANI, "Dynamic Compression of Cellular Cores: Temperature and Strain Rate Effects". *Comp. Struct.* **58**(4) (2002) 505.
6. S. LOPATNIKOV, B. GAMA, J. HACQUE, C. KRAUTHAUSER, J. GILLEPSIE, M. GUDEN and I. HALL, "Dynamics of Metal Foam Deformation During Taylor Cylinder-Hopkinson bar Impact Experiment" *Comp. Str.* **61**(1–2) (2003) 61.
7. CH. LALANNE, "Chocs mécaniques", Edition Hermes, Chap. 6, ISBN 2-7462-0034-1.
8. M. LAMBERT *et al*., "High Strain Rate Testing of Aluminium Alloy and High Speed Photography", dymat 2003, Porto, ed. EDP Sciences, pp. 543-549, ISBN 2-86883-696-8.
9. P. VIOT and F. BEANI, "Polypropylene Foam Behavior Under Compressive Loading at High Strain Rate" 8e International Conference on Structures Under Shock and Impact, Crete, Greece, 2004. ED. Witpress, pp. 507–516. ISBN 1-85312-706-X.
10. M. AVALLE *et al*., "Characterization of Polymeric Structural Foam Under Compressive Impact Loading by Means of Energy-Absorption Diagram" *Int. J. Imp. Engg.* **25** (2001) 455.
11. R. TIE BI, N. BRETAGNE and J. C. DUPRÉ, "Mesures par suivi de marqueurs et thermographie infrarouge de paramètres thermomécaniques" colloque photomécanique "étude du comportement des matériaux et des structures", 2001, Poitiers.ED. GAMAC, pp 143–150 ISBN : 2-951-636-80-6.
12. VACHER DUMOULIN and MORESTIN MGUIL-TOUCHAL, "Bidimensional Deformation Measurement Using Digital images," *Proc. Inst. Mech. Eng.* **213** (1999), 811.
13. S. MGUIL-TOUCHAL, F. MORESTIN and M. BRUNET, "Various experimental applications of digital image correlation method", in CMEM 97 (Computational Methods and Experimental Measurements VIII) (Rhodes, 1997) p 46.

Received December 2004
and accepted April 2005